1550 nm InGaAs/InAlAs single photon avalanche diode at room temperature

Xiao Meng, Chee Hing Tan, Simon Dimler, John P R David, and Jo Shien Ng*

Department of Electronic and Electrical Engineering, University of Sheffield, Sheffield S1 3JD, UK
** j.s.ng@sheffield.ac.uk*

Abstract: An InGaAs/InAlAs Single Photon Avalanche Diode was fabricated and characterized. Leakage current, dark count and photon count measurements were carried out on the devices from 260 to 290 K. Due to better temperature stability of avalanche breakdown in InAlAs, the device breakdown voltage varied by < 0.2 V over the 30 K temperature range studied, which corresponds to a temperature coefficient of breakdown voltage less than 7 mV/K. The single photon detection efficiency achieved in gated mode was 21 and 10% at 260 and 290 K, respectively. However the dark count rates were high due to excessive band-to-band tunneling current in the InAlAs avalanche region.

OCIS codes: (040.3060) Infrared; (250.1345) Avalanche photodiodes (APDs); (030.5260) Photon counting.

References and links

1. D. Stucki, G. Ribordy, H. Z. A. Stefanov, and J. G. Rarity, "Photon counting for quantum key distribution with peltier cooled InGaAs-InP APDs," J. Mod. Opt. **48**(13), 1967–1981 (2001).
2. A. L. Lacaita, P. A. Francese, and S. D. Cova, "Single-photon optical-time-domain reflectometer at 1.3 μm with 5-cm resolution and high sensitivity," Opt. Lett. **18**(13), 1110–1112 (1993).
3. S. Pellegrini, G. S. Buller, J. M. Smith, A. M. Wallace, and S. Cova, "Laser-based distance measurement using picosecond resolution time-correlated single-photon counting," Meas. Sci. Technol. **11**(6), 712–716 (2000).
4. F. Marsili, V. B. Verma, J. A. Stern, S. Harrington, A. E. Lita, T. Gerrits, I. Vayshenker, B. Baek, M. D. Shaw, R. P. Mirin, and S. W. Nam, "Detecting single infrared photons with 93% system efficiency," Nat. Photonics **7**(3), 210–214 (2013).
5. S. Pellegrini, R. E. Warburton, L. J. J. Tan, J. S. Ng, A. B. Krysa, K. M. Groom, J. P. R. David, S. Cova, M. J. Robertson, and G. S. Buller, "Design and performance of an InGaAs-InP single-photon avalanche diode detector," IEEE J. Quantum Electron. **42**(4), 397–403 (2006).
6. M. A. Itlzer, X. Jiang, M. Entwistle, K. Slomkowshi, A. Tosi, F. Acerbi, F. Zappa, and S. Cova, "Advances in InGaAsP-based avalanche diode single photon detectors," J. Mod. Opt. **58**(3–4), 173–200 (2011).
7. Y. Liang, Y. Jian, X. Chen, G. Wu, E. Wu, and H. Zeng, "Room-temperature single-photon detector based on InGaAs/InP avalanche photodiode with multichannel counting ability," IEEE Photon. Technol. Lett. **23**(2), 115–117 (2011).
8. G. Karve, X. Zheng, X. Zhang, X. Li, S. Wang, F. Ma, A. Holmes, J. C. Campbell, G. S. Kinsey, J. C. Boisvert, T. D. Isshiki, R. Sudharsanan, D. S. Bethune, and W. P. Risk, "Geiger mode of an $In_{0.53}Ga_{0.47}As$–$In_{0.52}Al_{0.48}As$ avalanche photodiodes," IEEE J. Quantum Electron. **39**(10), 1281–1286 (2003).
9. T. Nakata, E. Mizuki, T. Tsukuda, S. Takahashi, H. Hatakeyama, T. Anan, K. Makita, and A. Tomita, "InAlAs avalanche photodiodes for gated Geiger mode single photon counting," in *Proceeding of 15th OptoElectronics and Communications Conference*, (IEEE, 2010), pp. 822–823.
10. K. Zhao, S. You, J. Cheng, and Y. Lo, "Self-quenching and self-recovering InGaAs/InAlAs single photon avalanche detector," Appl. Phys. Lett. **93**(15), 153504 (2008).
11. L. J. J. Tan, D. S. G. Ong, J. S. Ng, C. H. Tan, S. K. Jones, Y. H. Qian, and J. P. R. David, "Temperature dependence of avalanche breakdown in InP and InAlAs," IEEE J. Quantum Electron. **46**(8), 1153–1157 (2010).
12. S. C. Liew Tat Mun, C. H. Tan, S. J. Dimler, L. J. J. Tan, J. S. Ng, Y. L. Goh, and J. P. R. David, "A theoretical comparison of the breakdown behavior of $In_{0.52}Al_{0.48}As$ and InP near-infrared single-photon avalanche photodiodes," IEEE J. Quantum Electron. **45**(5), 566–571 (2009).
13. S. Wang, F. Ma, X. Li, G. Karve, X. Zheng, and J. C. Campbell, "Analysis of breakdown probabilities in avalanche photodiodes using a history-dependent analytical model," Appl. Phys. Lett. **82**(12), 1971–1973 (2003).

#210354 - $15.00 USD Received 12 Jun 2014; revised 1 Sep 2014; accepted 1 Sep 2014; published 11 Sep 2014

14. D. A. Ramirez, M. M. Hayat, G. Karve, J. C. Campbell, S. N. Tores, B. E. A. Saleh, and M. C. Teich, "Detection efficiencies and generalized breakdown probabilities for nanosecond-gated near infrared single photon avalanche photodiodes," IEEE J. Quantum Electron. **42**(2), 137–145 (2006).
15. B. F. Levine, C. G. Bethea, and J. C. Campbell, "Near room temperature 1.3 μm single photon counting with a InGaAs avalanche photodiode," Electron. Lett. **20**(14), 596–597 (1984).
16. D. A. Humphreys, R. J. King, D. Jenkins, and A. J. Moseley, "Measurement of absorption coefficients of $Ga_{0.47}In_{0.53}As$ over the wavelength range 1.0-1.7 μm," IEE Electronic Lett. **21**(25/26), 1188–1189 (1985).
17. Y. Zhang, X. Zhang, and S. Wang, "Gaussian pulse gated InGaAs/InP avalanche photodiode for single photon detection," Opt. Lett. **38**(5), 606–608 (2013).
18. Y. L. Goh, D. J. Massey, A. R. J. Marhsall, J. S. Ng, C. H. Tan, W. K. Ng, G. J. Rees, M. Hopkinson, J. P. R. David, and S. K. Jones, "Avalanche multiplication in InAlAs," IEEE Trans. Electron. Dev. **54**(1), 11–16 (2007).

1. Introduction

Single Photon Avalanche Diodes (SPADs) sensitive to 1550 nm wavelength light are important for a number of applications, e.g. quantum key distribution [1], time-resolve spectroscopy [2], and laser-ranging [3]. Despite progress in devices such as Superconducting Single Photon Detectors [4], SPADs remain the preferred single photon detectors, largely because they operate within the temperature range achievable by thermoelectric coolers.

Based on planar device structure of telecommunication avalanche photodiodes (APDs), the current SPADs use InGaAs and InP for their absorption region and avalanche region, respectively [5–7]. Guard ring and double zinc-diffusion (to define the p-region), as in those used in InGaAs/InP APDs, are employed to suppress edge breakdown in these SPADs. Early custom-designed InGaAs/InP SPADs demonstrated a Single Photon Detection Efficiency (*SPDE*) of 10% at 200 K [5], which was later improved to *SPDE* of 20% at 215 K [6]. Liang *et al.* operated an InGaAs/InP SPAD with capacitance balancing circuit (to cancel the capacitive transients which often interfere with detection of avalanche signals) and reported a *SPDE* of 9.8% and negligible after-pulsing at 290 K [7]. However no information on the design and device fabrication of the SPAD used was given. Still, operating the SPADs at or close to room temperature whilst maintaining reasonable *SPDE* is very attractive. There is an obvious advantage in terms of less complicated and hence cheaper device packaging. Operating at high temperatures also reduces the severity of after-pulse problem, which tends to worsen as temperature decreases.

Various groups reported APDs and SPADs using InAlAs, instead of InP, for the avalanche region [8–10]. The first InGaAs/InAlAs SPAD, reported by Karve *et al*. [8], exhibited *SPDE* of 16% at 130 K. Nakata *et al.* [9] achieved better overall performance with *SPDE* of 10% at 213 K, which was probably partially due to the much smaller SPAD diameter (20 μm, which is typical in recent SPADs) than that in Karve *et al.* (160 μm). A self-quenching InGaAs/InAlAs SPADs operated in sub-Geiger mode was also demonstrated by Zhao *et al.* in [10] and they exhibited *SPDE* between 6 and 14% at 240 to 120 K.

With the majority of recent reports using InGaAs/InP SPADs, the research focus of 1550 nm SPADs had reverted back to InGaAs/InP SPADs, even though InGaAs/InAlAs APDs are now established technology for APDs. Yet, replacing InP with InAlAs as the avalanche region material could offer a number of advantages for SPADs. Firstly the temperature stability of avalanche breakdown voltage, V_{bd}, is better in InAlAs that in InP [11]. This affords greater freedom in adjusting the operation temperature of SPADs for optimum operation as well as less stringent voltage control for the SPADs. For example, a SPAD with a 2.5 μm absorber and a 1.0 μm avalanche region (as from [5]) has a temperature coefficient of avalanche breakdown voltage, C_{bd}, of 151 or 57 mV/K, depending on whether the avalanche region is made of InP or InAlAs, as predicted using Eqs. (1) and 2 from [11]. Note that for a given avalanche material, a design with a narrow avalanche region will yield a smaller C_{bd} than one with a thick avalanche region.

Secondly, InAlAs SPADs have potentially higher *SPDE*, which is directly proportional to avalanche breakdown probability, P_b, than InP SPADs. It is well established that P_b rises more rapidly with overbias ratio, defined as $(V - V_{bd})/V_{bd}$, in InAlAs than in InP [12–14].

#210354 - $15.00 USD Received 12 Jun 2014; revised 1 Sep 2014; accepted 1 Sep 2014; published 11 Sep 2014

Using 1.0 μm avalanche region as an example, P_b at 5% overbias ratio is 0.72 and 0.58 for InAlAs and InP, respectively, with larger differences at smaller overbias ratio [12].

Thirdly APDs and SPADs using InAlAs have been developed using the mesa structure. Mesa structures can be scaled more easily to linear and 2-dimensional arrays with small pitch, compared to planar structure. They offer much simpler design as guard ring and double dopant diffusion are not required to suppress edge breakdown.

In order to take advantage of the benefits associated with InAlAs avalanche region, we demonstrate here an InGaAs/InAlAs SPAD for 1550 nm detection. Dark count and photon counting data of the SPAD with mesa structure operated at temperatures ranging from 260 K to room temperature are presented.

2. Experimental details

Nominal wafer details of our InGaAs/InAlAs SPAD are shown in Fig. 1. It was grown by molecular beam epitaxy (MBE) on a semi-insulating InP substrate at the EPSRC National Centre for III-V Technologies at the University of Sheffield. The wafer consisted of a 600 nm InGaAs absorption region and a 200 nm InAlAs avalanche region. An InAlAs charge sheet layer between the avalanche and absorption regions ensured high and low electric fields across the respective layers. Two 50 nm InAlGaAs grading layers were utilized to reduce trapping of carriers at the InGaAs/InAlAs heterojunctions. The p^+ buffer layer has a highly doped 10 nm top InGaAs contact layer and a 300 nm p-type InAlAs cladding layer. The thin InGaAs contact layer ensures good ohmic contact without attenuating the incident light significantly. The n^+ buffer layer consisted of a 100 nm n-type InAlAs cladding layer and a 300 nm n-type InGaAs layer.

The absorption and avalanche regions are narrower compared to the designs of InGaAs/InP SPADs in [5] and [6]. This allows us to achieve very small C_{bd}, by minimizing both the avalanche region width and the total depletion region width (made up of the avalanche region, absorption region, grading, and charge sheet). The narrow absorption region also makes it easier to achieve sufficiently low surface leakage currents from mesa devices, although these advantages are at the expense of absorption efficiency.

p+: InGaAs contact
p+: InAlAs cladding
i : InAlGaAs grading
i : InGaAs, 600 nm
i : InAlGaAs grading
p+: InAlAs charge sheet
i : InAlAs, 200 nm
n+: InAlAs cladding
n+: InGaAs contact
InP semi-insulating substrate

Fig. 1. Structure details of InGaAs/InAlAs SPAD.

Mesa devices with diameters of 25 to 100 μm were fabricated from the wafer using standard photolithography and wet chemical etching with a solution of sulphuric acid: hydrogen peroxide: deionized water (ratio of 1:8:80). The p-contacts and n-contacts were formed by annealed metals of Ti/Pt/Au and In/Ge/Au, respectively. The devices were passivated by silicon nitride. The mesa devices had Ti/Pt/Au p-bondpads that were deposited on the semi-insulating substrate. The vast majority of the results shown in Section 3 were obtained from the 25 μm diameter SPADs, which had low bulk dark currents and junction capacitance. No anti-reflection coating was employed.

Capacitance-Voltage (C-V) measurements of the mesa devices were carried out at room temperature using a HP4275 LCR meter. Current-Voltage (I-V) measurements of the devices

#210354 - $15.00 USD Received 12 Jun 2014; revised 1 Sep 2014; accepted 1 Sep 2014; published 11 Sep 2014

at temperatures ranging from 260 to 290 K were performed using a Janis ST-500 probe station connected to a Keithley Model 236 source-measure-unit. To obtain dark current and photocurrent data, the I-V measurements were conducted in the dark and with fibre-coupled continuous-wave (CW) 1550 nm light from an Agilent 8164A tunable laser source, respectively.

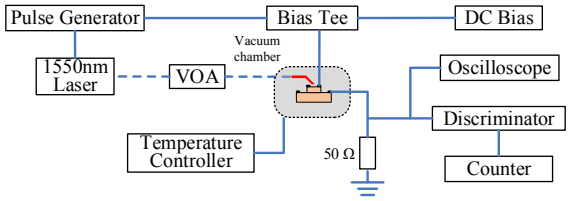

Fig. 2. Experimental setup for dark counts and photon counts measurements. Solid lines and dashed lines represent electrical and optical connections, respectively.

For dark counts and photon counts measurements, the device-under-test was operated in gated mode, as is common for SPADs sensitive to 1550 nm lights. The setup used is shown schematically in Fig. 2 and the SPAD was again placed inside the Janis probe station. In order to pulse-bias the SPAD above the breakdown voltage, a commercial bias tee (Picosecond Pulse Labs, 5530B) was used to superimpose AC voltage pulses on a DC bias, which is set below the breakdown voltage. The AC voltage pulses was provided by an Avtech AVI-V-2L pulse generator and had 1.2 ns pulse width (full-width at half-maximum), 6 V pulse height, and 100 kHz repetition frequency, unless otherwise stated. The fixed AC voltage pulses ensured constant AC pulse width for all measurements. Avalanche signals from the SPAD (due to dark or photon-generated carriers) were detected by an edge-triggered discriminator, which then generated nuclear instrument module (NIM) signals. The NIM signals were supplied to a Canberra 512 counter to yield count rate. The avalanche signals were also monitored using a Lecroy Waverunner 204Xl oscilloscope during measurements.

Photon source for the photon counts measurements was a fibre-coupled pulsed laser from Picosecond Laser Diode Systems, which emits 1550 nm wavelength light pulses with 20 ps pulse width (full-width at half-maximum) at a frequency of 100 kHz. The light pulses were synchronized with the voltage pulse (also at 100 kHz) and was attenuated to a desired level by an Exfo FVA-3100 variable optical attenuator (VOA). The optical attenuator's attenuation settings relevant to this work were confirmed through separate optical power measurement using a commercial InGaAs photodiode and the CW 1550 nm laser.

Optical coupling efficiency from the fibre to a 25 μm diameter SPAD, η, was determined to be 5%, through separate optical power measurements using the CW 1550 nm laser and photodiodes with known responsivity. In photon count measurements, the average number of photons arriving at the diode per pulse can be estimated using $N = \eta\ P_{average} / (f\ hv)$, where $P_{average}$ is the average power of laser at the end of the fiber, h is the Planck's constant, v is the frequency of the incoming photon, and f is repetition frequency of the pulsed laser. With η = 0.05, $P_{average}$ = 77 fW, photon energy = 0.8 eV, and f = 100 kHz, there was an average of 0.3 photon per pulse.

Assuming Poissonian statistics for the arriving photons, *SPDE* can be expressed as [15]

$$SPDE = \frac{1}{N}\ln\left(\frac{1-P_d}{1-P_t}\right), \tag{1}$$

where P_t and P_d are the measured probability of having an avalanche event for a pulse when the SPAD is illuminated with the photon pulses and in the dark, respectively. P_t was obtained experimentally from the ratio of count rate taken with the photon pulses to f. P_d was similarly given by the ratio of count rate taken in the dark to f. Dark count rate is defined as the count

#210354 - $15.00 USD Received 12 Jun 2014; revised 1 Sep 2014; accepted 1 Sep 2014; published 11 Sep 2014

rate in the dark divided by the product of voltage pulse width and *f*, which will enable comparisons to be made with results from other reports using different voltage pulse width and *f*.

3. Results

Typical dark current and photocurrent (1550 nm light) data of a 25 μm diameter SPAD at temperatures from 260 to 290 K are shown in Fig. 3. The photocurrent data showed similar punch-through voltages (~15 V) at different temperatures. Within the temperature range studied, the breakdown voltages indicated by dark current data varied by < 0.2 V, consistent with the small C_{bd} expected from [11]. Thus, there was always at least 10 V difference between the breakdown voltage and punch-through voltage, ensuring that the absorption region of SPAD is fully depleted even at low temperature. The dark current at 90% of breakdown voltage was 54 and 120 nA at 260 and 290 K, respectively. Also included in Fig. 3 is the room temperature leakage current of a 25 μm diameter diode without p-bondpad (from the same sample piece), which is at least an order of magnitude lower than that of the tested diode. This indicates that leakage current due to bondpads contributed significantly to the measured leakage current of the tested diode, but this is not expected to affect dark counts.

C-V data at 290 K are shown in Fig. 4(a). These were obtained from the largest diodes (100 μm diameter), in order to maximize accuracy in the measurement. By fitting to the C-V data using an electrostatic model and assuming abrupt changes in doping density from layer to layer, an estimated doping profile of our SPAD was obtained. The fitting is also shown in Fig. 4(a). The experimental capacitance data decreased rapidly with reverse bias at ~15 V, because of the depletion of absorption region. This is consistent with the increase in photocurrent at ~15V (Fig. 3). Using the estimated doping profile, an electric field profile was calculated for reverse bias of 26 V (the breakdown voltage at 290 K), as shown in Fig. 4(b).

SPDE and *DCR* data as functions of DC bias obtained from the SPAD at 260 to 290 K, using a fixed AC pulse height of 6 V, are shown in Figs. 5(a) and 5(b), respectively. *SPDE* of 10% at 290 K and 21% at 260 K were achieved. Observing Fig. 5(b), for a given DC bias, the *DCR* increased slightly as temperature decreased.

Since SPADs sensitive to 1550 nm light can suffer from significant after-pulse problem, dark counts measurements were repeated at room temperature for *f* ranging from 1 to 100 kHz (the maximum repetition frequency of the pulse generator). The data for 4.5 V overbias (24.5 V DC with 6 V AC bias) are shown in Fig. 6. No significant dependence on frequency could be observed, confirming after-pulsing is not the dominant source of the dark counts within this temperature range.

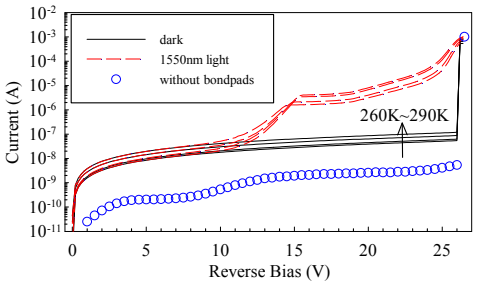

Fig. 3. Reverse dark current and photocurrent (1550nm light) data of a 25 μm diameter InGaAs/InAlAs SPAD at 260 to 290 K. Dark current of a diode without p- bondpad at room temperature is also shown (circle).

#210354 - $15.00 USD Received 12 Jun 2014; revised 1 Sep 2014; accepted 1 Sep 2014; published 11 Sep 2014

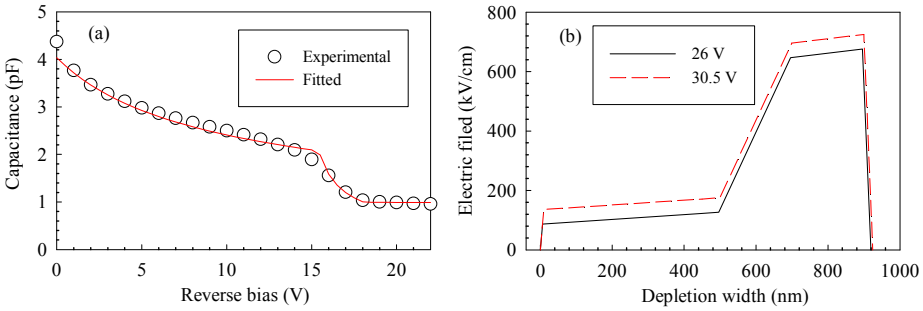

Fig. 4. (a) C-V data and fitting for a 100 μm diameter InGaAs/InAlAs SPAD. (b) Calculated electric field profiles at 26 and 30.5 V.

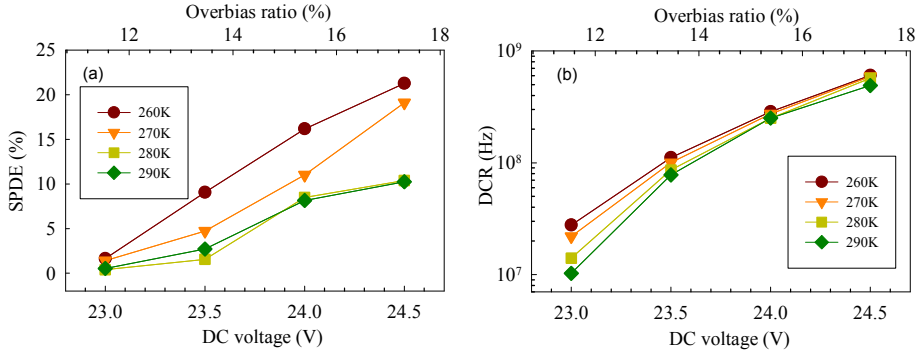

Fig. 5. (a) *SPDE* and (b) *DCR* versus DC bias (bottom horizontal axis) and overbias ratio (top horizontal axis) for the SPAD at 260 to 290 K. AC pulses with height of 6V and width of 1.2 ns were used.

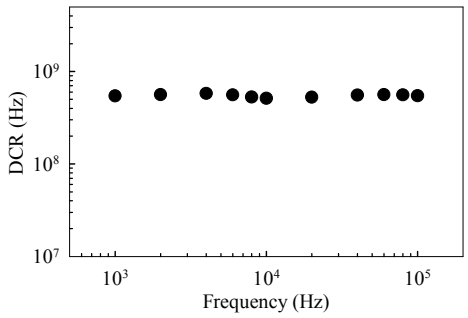

Fig. 6. *DCR* of the SPAD versus voltage AC pulse repetition frequency at room temperature with 4.5 V overbias. No after-pulse problem was observed.

4. Discussion

Our *SPDE* values are significantly higher than the *SPDE* values previously reported for InGaAs/InAlAs SPADs [8–10], and are approaching or exceeding those for InGaAs/InP SPADs [5–7], as shown in Fig. 7. Thus, mesa structure InGaAs/InAlAs SPADs represent a practical alternative to InGaAs/InP SPADs. The former may be particularly advantageous for development of dense arrays of SPADs.

#210354 - $15.00 USD Received 12 Jun 2014; revised 1 Sep 2014; accepted 1 Sep 2014; published 11 Sep 2014

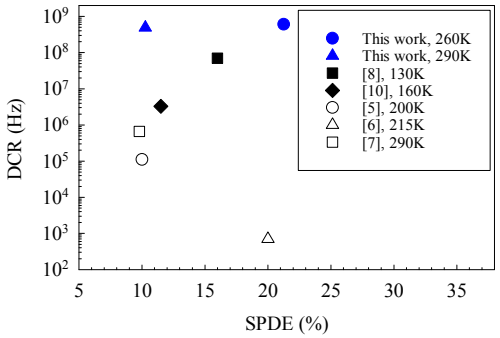

Fig. 7. *DCR* vs *SPDE* results in this work compared with previous reports of InGaAs/InAlAs (closed symbols) and InGaAs/InP SPADs (open symbols).

Absorption efficiency, P_{abs}, for a 600 nm InGaAs absorption layer is estimated at 0.39, assuming absorption coefficient of 0.82 μm^{-1} at 1550 nm [16]. Since *SPDE* is the product of P_{abs}, P_b, and (1 - P_{loss}), where P_{loss} is the probability that photo-generated carriers are lost before entering the avalanche layer. The small difference between the estimated P_{abs} and the highest measured *SPDE* (0.10) at 290 K suggests small P_{loss} and/or high P_b at the operating conditions used. This is supported by the P_b ~0.4 to 0.5 for a 200 nm InAlAs avalanche layer predicted for the conditions used to achieve *SPDE* of 21% [12].

The *DCR* of this work is higher than those for prior works on InGaAs/InAlAs SPADs, namely [8] (7×10^7 s^{-1} at 130 K) and [9] (3×10^6 s^{-1} at 160 K), as well as for the *DCR* reported for InGaAs/InP SPADs (e.g. ~10^4 s^{-1} at 253 K from [17]). There was no sufficient information in [9] to extract its *DCR*. The *DCR* data of our SPAD are insensitive to changes in temperatures within the range studied. This suggests that the dominant mechanism is unlikely to be diffusion or generation recombination current, both of which increase exponentially with temperature. Band-to-band tunneling current, which depends weakly on temperature, is thus a possible significant source of dark carrier generation.

In order to assess the significance of band-to-band tunneling current in our SPAD, electric field profile at 30.5 V, the maximum voltage applied in the dark count measurements, was calculated using the estimated doping profile as described in Section 3. This is shown in Fig. 4(b), along with the electric field profile at 26 V. The peak electric field in the InAlAs avalanche layer reaches 725 kV/cm at 30.5 V. Such fields were shown to cause significant tunneling current for a 200 nm InAlAs avalanche layer [18]. Hence the high *DCR* of our SPAD is attributed to excessive tunneling current from the InAlAs avalanche layer.

From Fig. 5(b), for a given bias condition, *DCR* was observed to increase marginally as temperature decreases. This is likely to be the result of competing effects on *DCR* from tunneling current and avalanche breakdown probability. As temperature decreases, the band-to-band tunneling current in the InAlAs layer decreases slightly, because the semiconductor material bandgap increases slightly (increasing the tunneling barrier height). However, as temperature decreases, V_{bd} of the SPAD decreases slightly, which may result in a slight increase in P_b and hence *DCR*, for a given voltage.

5. Conclusion

Mesa structure SPADs using InGaAs absorption region and InAlAs avalanche region were demonstrated to have good temperature stability (< 0.2 V change over 30 K). In gated mode, the *SPDE* of 10% and 21% was achieved at 290 K and 260 K, respectively. However high *DCR* over the temperature range studied was observed and was attributed to excessive tunneling current in the InAlAs avalanche layer. No noticeable after-pulse problem was observed in the frequency range (upto 100 kHz) studied. Overall the results indicate InGaAs/InAlAs has considerable potential for operation at (or near) room temperature.

#210354 - $15.00 USD Received 12 Jun 2014; revised 1 Sep 2014; accepted 1 Sep 2014; published 11 Sep 2014

Acknowledgments

This work is supported by the UK Engineering and Physical Sciences Research Council (EPSRC) under grants EP/D064759/1 and EP/K001469/1. The work of J. S. Ng was supported by the Royal Society University Research Fellowship.

#210354 - $15.00 USD Received 12 Jun 2014; revised 1 Sep 2014; accepted 1 Sep 2014; published 11 Sep 2014